Structural stability of (Ga,Mn)As from first principles: Random alloys, ordered compounds, and superlattices

Jorge Osorio-Guillén, Yu-Jun Zhao, Sergey V. Barabash, and Alex Zunger*
National Renewable Energy Laboratory, Golden, Colorado 80401, USA
(Received 19 September 2005; published 7 July 2006)

We calculate by a combination of density functional theory and mixed-basis cluster expansion the structural stability of ordered and disordered zincblende GaAs-MnAs systems. We find that the ground state of this system is phase separating into GaAs+MnAs, even though the strain energy is negligible. The study of short-period superlattices shows that the least-unstable superlattices are along the (111) orientation whereas the most-unstable orientation is the (201). The formation enthalpy of the random alloy has been calculated; combining it with a mean-field approximation, we obtain the temperature-composition phase diagram showing the miscibility-gap temperature below which the alloy phase separates. The stabilization energy for (100) $(Ga_{1-x}Mn_xAs)_1/(GaAs)_n$ superlattices shows that these superlattices prefer ferromagnetic order over a nonferromagnetic arrangement. Remarkably, the decay of the exchange interactions with superlattice period n is slower for the Mn dilute $x=0.5$ case than for $x=1$. This shows that as the system becomes more Mn dilute the range of the exchange interactions increase. This reveals an exceptional property of dilute magnetic semiconductors, namely that the system counter balances dilution of the magnetic ions by extending the range of exchange interactions, hence maintaining ferromagnetism down to small concentrations of a magnetic ion.

DOI: 10.1103/PhysRevB.74.035305 PACS number(s): 68.65.Cd, 64.75.+g, 71.15.Mb, 75.50.Pp

I. INTRODUCTION

Since the discovery[1–3] that *disordered substitution* of Mn ions on the cation site of III-V semiconductors produces ferromagnetism, numerous attempts were made at *ordered* substitutions,[4–12] examining both experimentally[4–8] and theoretically[9–12] the possibilities that superstructures $(Ga_xMn_{1-x}As)_n/(GaAs)_m$ grown along some directions $\hat{\mathbf{G}}$ will offer even better magnetic properties. Here we study theoretically the thermodynamic stability of such *superlattices*, as well as that of *ordered* $Ga_nMn_mAs_{n+m}$ compounds and $Ga_xMn_{1-x}As$ *random alloys*, using first-principles total-energy methods.[13] Our study is based on the zincblende lattice, even though pure MnAs has the NiAs structure, since, the *alloy* can be grown zincblende to $x \leqslant 0.5$.[4–8] Since there are as many as 2^N possible configurations of two atom types (Ga, Mn) substituting N fcc sites of the GaAs cation sublattice, one cannot use a direct calculation of all configurations. Yet, it is interesting to know which of the 2^N configuration has the lowest total energy (or which one is the least unstable). Furthermore, we wish to identify which superlattice parameters $(n,m,\hat{\mathbf{G}})$ provide the stablest (or least unstable) structures.[14] We thus use a Cluster Expansion (CE) approach,[15–18] in which $M \ll 2^N$ directly calculated energies $E_{\text{direct}}(\sigma)$ are performed on M ordered atomic configurations σ of $Ga_nMn_mAs_{n+m}$. The resulting set of formation enthalpies $\{\Delta H_{\text{direct}}(\sigma)\}$ is mapped onto a generalized Ising-like expansion,

$$\Delta H_{\text{CE}}(\sigma) = J_0 + \sum_i J_i \hat{S}_i + \sum_{ij}^{\text{All pairs}} J_{ij}\hat{S}_i\hat{S}_j + \sum_{ijk}^{\text{All 3 bodies}} J_{ijk}\hat{S}_i\hat{S}_j\hat{S}_k + \cdots, \quad (1)$$

where $\hat{S}_i$ denotes if site $i=1,\ldots,N$ is occupied by Ga ($S_i=+1$) or Mn ($S_i=-1$), and $\{J\}$ are unknown interaction energies that can extend, in principle, to 2^N terms, but in practice a much smaller number of interactions are sufficient for accurate description of the alloy energetics.[16,17] Unlike the tradition in Ising expansions for magnetism[19] or alloys,[20–22] we do not feel that we can select *a priori* the numbers and type of terms entering the expansion Eq. (1). Instead, we have developed[15–17,23,24] a methodology that selects the number and type of "many-body interaction types" (MBITs) appearing in Eq. (1) according to the criteria that $\Delta H_{\text{CE}}(\sigma)$ not only *fit* $\{\Delta H_{\text{direct}}(\sigma)\}$ for M "input" structures, but that $\Delta H_{\text{CE}}(\sigma)$ also *predict* $\{\Delta H_{\text{direct}}(\sigma' \neq \sigma)\}$ for many sets $\{\sigma'\}$ of configurations not used in the fit. The techniques required to do this are briefly reviewed in Sec. II. Establishing the expansion Eq. (1) in this way for GaAs/MnAs turns out to require four pair-interactions and five many-body terms (which include two three-body and three four-body terms), and provides a precision of ≈ 2 meV/cation (while the typical formation enthalpy ΔH is of the order of ≈ 25 meV/cation). Once established, Eq. (1) can be used almost effortlessly to scan a large number of other configurations (in practice, $\approx 3\times 10^6$ structures), finding their energies. From such extensive structure scans we find the following

(i) The GaAs-MnAs zincblende system is phase separating, i.e., $\Delta H(\sigma) \geqslant 0$ for all σ at $T=0$. Thus, the ground state is GaAs+MnAs, or *infinite-period* $(MnAs)_\infty/(GaAs)_\infty$ superlattices.

(ii) Although ordinary *isovalent* lattice-mismatched zincblende superlattices such as $(InAs)_n/(GaAs)_m$ or $(GaP)_n/(InP)_m$ also have a phase-separating ground-state,[25] zincblende (MnAs)/(GaAs) is different: In the former, isovalent lattice-mismatched case $\Delta H(x) \geqslant 0$ largely because of the *strain* needed to bring the constituent binary components into a common lattice.[26] When strain is the cause of phase-separation, the order of long-period superlattice energies is[27,28]

$$(100) < (110) < (201) < (111). \quad (2)$$

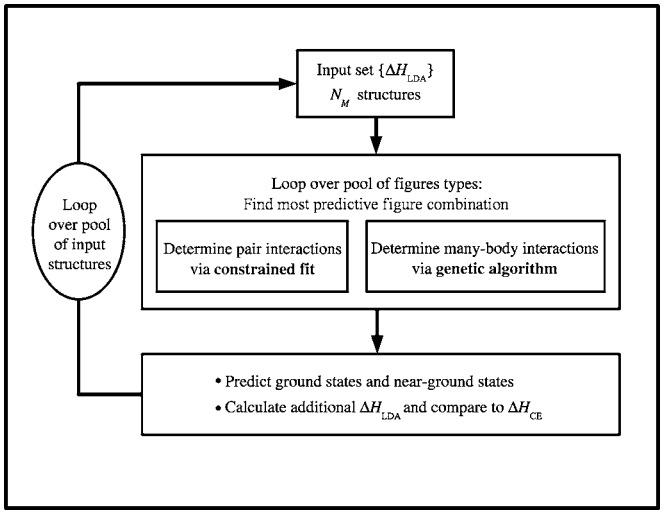

FIG. 1. Schematic flow chart of the procedure used to establish the cluster expansion.

In contrast, owing to the close match of the lattice parameters of zincblende GaAs and MnAs, here $\Delta H(x) \geqslant 0$ due to unfavorable chemical interactions, leading to a different order of stability, viz. Eq. (3) below.

(iii) Restricting ourself to short-period superlattices we find that the least-unstable ones correspond to the (111) orientation. The order of stability in the long-period limit is

$$(111) < (100) < (110) < (201). \tag{3}$$

(iv) We calculate $\Delta H(x)$ of the *random* $Ga_{1-x}Mn_xAs$ alloy, finding that

$$\Delta H_R(x) = \Omega_1 x(1-x) + \Omega_2 x^2(1-x) + \Omega_3 x^3(1-x)\cdots \tag{4}$$

is a good approximation to the first-principles result, with $\Omega_1 = 293$ meV, $\Omega_2 = -390$ meV, and $\Omega_3 = 239$ meV. The formation enthalpy of the random alloy has been calculated; combining it with a mean-field approximation, we obtain the temperature-composition phase diagram, showing the miscibility-gap temperature below which the alloy phase separates.

(v) The calculation of $E_{\mathrm{FM}} - E_{\mathrm{AFM}}$ vs n for $(Ga_{1-x}Mn_xAs)_1/(GaAs)_n$ superlattices along the direction (100) with $x = 0.5, 1$ and $n = 1, 2, \ldots, 6$ shows that these superlattices prefer a ferromagnetic order. The exchange interactions decay with superlattice period n more strongly for $x = 1$ than $x = 0.5$. Thus, in the dilute superlattices the exchange interaction becomes long range. This reveals an exceptional property of dilute magnetic semiconductors, namely that the system counterbalances dilution of the magnetic ions by extending the range of exchange interactions (not to be confused with the chemical interactions $\{J\}$), hence maintaining ferromagnetism down to small concentrations of a magnetic ion.

II. METHOD OF ESTABLISHING THE CLUSTER EXPANSION

We expand[17] $\Delta\tilde{H}_{\mathrm{direct}} = \Delta H_{\mathrm{direct}} - E_{\mathrm{ref}}$ by $\Delta\tilde{H}_{\mathrm{CE}}$, where

$$\Delta\tilde{H}_{\mathrm{CE}} = \Delta H_{\mathrm{CE}} - E_{\mathrm{ref}} = J_0 + (2x-1)J_1 + \sum_{\mathrm{pairs}} J_{\mathrm{pair}} D_{\mathrm{pair}} \bar{\Pi}_{\mathrm{pair}}(\sigma) + \sum_{\mathrm{MBITs}} J_{\mathrm{MB}} D_{\mathrm{MB}} \bar{\Pi}_{\mathrm{MB}}(\sigma). \tag{5}$$

The first sum includes symmetry equivalent pairs and the second sum includes many-body interaction types (MBITs) f. The interaction parameters J_f are unknown energies that are found by a fitting procedure. D_f is the number of interactions belonging to the interaction type f per site, and $\bar{\Pi}_f$ is space-averaged spin products over the sites that make up the MBIT f. As a reference energy E_{ref}, we use the constituent strain (CS) energy[17] ΔE_{CS}, representing the strain energy associated with deforming the constituent solids A and B to their structure within the compound. Subtracting this term before the expansion accelerates the convergence and fixes the shortcoming of simpler expansions,[18] which predict the formation enthalpies of long-period superlattices going to zero in the long-period limit. Although Eq. (5) contain, in principle, 2^N interaction parameters, the energetics of the bonding is usually determined by fewer interactions. Then, we can truncate the expansion Eq. (5), and find a finite set of interaction parameters $\{J\}$ that provide an accurate mapping of the energetics of the system. These J_f are obtained from a set of formation enthalpies $\Delta H_{\mathrm{direct}}(\sigma) = \Delta H_{\mathrm{GGA}}(\sigma)$ calculated by first-principle total energy using Density Functional Theory (DFT) in the generalized gradient approximation (GGA). We use an iterative scheme (see Fig. 1) to find the J_f's as follows:

We build the CE not only on the ability to fit energies, but on its ability to predict energies of structures that were not fitted.[29] To do so, we divide the set of N_M input structures into two groups: One used to fit ("fitting set") and one used to test predictions ("prediction set"). There are N_P prediction subsets made of N_V structures. The selection of MBITs is based on a cross-validation (CV) score,[30] specifically the leave-many-out CV technique,[23] where the CV score is the average prediction error over the different N_P prediction subsets:

$$S_{\mathrm{cv}} = \frac{1}{N_P N_V} \sum_{i}^{N_P} \sum_{\mathrm{pred.\ set}\ i} |\Delta\tilde{H}^{(i)}_{\mathrm{GGA}} - \Delta\tilde{H}_{\mathrm{CE}}|^2. \tag{6}$$

Finding the pair interactions: We cast pair interaction in reciprocal space,

$$\sum_{\mathrm{pairs}} J_{\mathrm{pair}} D_{\mathrm{pair}} \bar{\Pi}_{\mathrm{pair}} = \sum_{\mathbf{k}} J_{\mathrm{pair}}(\mathbf{k}) |S(\mathbf{k},\sigma)|^2, \tag{7}$$

where the structure factor $S(\mathbf{k},\sigma) = (1/N)\Sigma_l^N S_l(\sigma) e^{i\mathbf{k}\cdot\mathbf{R_l}}$ is a lattice Fourier transform of spin-occupation variables and the sum extends on wave vectors $\mathbf{k}$ for which $S(\mathbf{k},\sigma)$ is nonzero. To ensure that only those pair interactions that improve the fit of ΔH_{CE} to ΔH_{GGA} enter, we add a Lagrange multiplier to our least-squares fit, which requires "maximum smoothness" to $J(\mathbf{k})$, the Fourier transform of the real space J_{pair}. This is obtained by minimizing

TABLE I. Directly calculated GGA formation enthalpies (meV/cation) and cluster expansion (CE) values for structures not used in the fit (pure predictions). Supercells are built on the zincblende simple cubic conventional cell and the face center cubic primitive cell are denoted by sc and fcc, respectively. SQS-14 denotes a special quasirandom structure that mimics the random alloy.

Formula	$Ga_{31}Mn_1$	$Ga_{26}Mn_1$	$Ga_{30}Mn_2$				$Ga_{56}Mn_2$	Ga_5Mn_1	Ga_6Mn_2
x_{Mn}	0.03125	0.037	0.0625				0.125	0.167	0.25
Supercell	$2\times2\times2$ sc	$3\times3\times3$ fcc	1NN	$2\times2\times2$ sc 2NN	3NN	4NN	$4\times4\times4$ fcc	(100)	SQS-14
Direct	9.78	10.02	14.08	19.10	16.76	15.44	27.45	23.44	42.04
CE	9.07	10.77	16.03	18.39	17.34	16.65	29.04	22.16	41.32

$$\sum_{\sigma\notin \text{pred. set}} |\Delta\tilde{H}_{\text{GGA}} - \Delta\tilde{H}_{\text{CE}}|^2 + \frac{t}{\alpha}\sum_{\mathbf{k}} J(\mathbf{k})(-\nabla_{\mathbf{k}}^2)^{\lambda/2} J(\mathbf{k})$$
$$= \sum_{\sigma\notin \text{pred. set}} |\Delta\tilde{H}_{\text{GGA}} - \Delta\tilde{H}_{\text{CE}}|^2 + \frac{N}{2\alpha}\sum_{\text{pair}} R_{\text{pair}}^{\lambda} D_{\text{pair}} J_{\text{pair}}^2, \tag{8}$$

where the first term is the usual least square and the second term allows a "$t-\lambda$" constrained fit that enforces the spatial decay of J_{pair} in terms of pair distance R_{pair}, with t being a Lagrangian multiplier and α being a normalization constant.[17]

Finding many-body interactions: We first define a large set $\mathcal{O}(10^2)$ of MBITs that contain three-body, four-body, five-body, and six-body figures. This set includes many more terms than we eventually use. The choice of an optimal small MBIT combination from the large set, it is done by the Generic Algorithm[24] (GA). The GA starts from initial trial combinations (*genomes*) of a fixed number of many-body figures. Each genome is represented by a string that contains one or zero (*genes*) depending on if the MBIT is or is not included in Eq. (8). The GA works in an iterative fashion: From the initial trial generation of genomes, by means of mating, we generate a new generation of trial genomes. This new generation contains newly generated children genomes that replace those parent genomes that produced a poor (high) CV score in the previous generation. These new genomes are then mated again and allowed to mutate in order to get the next generation of trial genomes, and so on. The genomes that produce the best CV score are kept during the next generations and are replaced gradually by better genomes. We say that GA has found a candidate CE when a genome with the best CV scores has not been replaced by a better one after a certain number n_{lockout} of generations, in which case that genome is prohibited from appearing again ("locked-out") and a new set of genomes is randomly generated to continue the GA search. This helps GA find the true global minimum and avoid spending too much time trying to escape local minima.[31]

The two steps above pertain to one set of input structures (the "internal loop" in Fig. 1). As Fig. 1 shows, once we have a CE we need to examine its ground state structures, and if some of them were not in the "input set," we need to calculate their GGA energy $\Delta\tilde{H}_{\text{GGA}}$ and add them as input and continue with the "outer loop." In practice, for GaAs -MnAs, we find only two ground states (isolated MnAs and GaAs), so there are no additional outer loop iterations. Instead, to ensure that the cluster expansion obtained after a single outer loop iteration accurately predicts the energies of arbitrary (Ga, Mn)As structures, we construct a set of other structures, never used in the fit, and use them for pure predictions.

In a mixed-basis cluster expansion, one normally subtracts from ΔH_{GGA} the reference energy E_{ref}, being the constituent strain (CS) energy. The latter is designed to cancel the singularity in[17] $J(\mathbf{k}\to 0)$. The key quantity in the calculation of the CS energy is the direction-dependent energy of infinite period A_∞/B_∞ superlattices,

$$\Delta E_{\text{CS}}(\sigma) = \sum_{\mathbf{k}} [(1-x)\Delta E_{\text{A}}^{\text{epi}}(\hat{k},a_\perp) + x\Delta E_{\text{B}}^{\text{epi}}(\hat{k},a_\perp)]|S(\mathbf{k},\sigma)|^2, \tag{9}$$

where

$$\Delta E_i^{\text{epi}}(\hat{k},a_\perp) = E_i^{\text{epi}}(\hat{k},a_\perp) - E_i^{\text{epi}}(\hat{k},a_i^{\text{eq}}) \tag{10}$$

is the *epitaxial deformation* energy of pure i=A,B, that is, the energy of pure i placed on a $\hat{k}$ substrate with the lattice constant $a_\perp = a_\perp(x)$ being the equilibrium lattice constant of the A_∞/B_∞ superlattice along $\hat{k}$. We found that in the case of (MnAs)/(GaAs) superlattices, the CS energy is less than 1 meV/cation. Since $\Delta E_{\text{CS}}(\sigma) \ll \Delta H_{\text{GGA}}(\sigma)$, we will neglect it.

More details about the method can be found in Refs. 15–17, 23, and 24.

III. RESULTS

A. The cluster expansion

The directly calculated energies of our input structures are shown in Table II: The structures are the GaAs and MnAs in the zincblende crystal structure, simple $Ga_nMn_mAs_{n+m}$ superlattices along the principal directions, and one zincblende supercell. To determine *pair interactions* of Eq. (1), we use the $\lambda-t$ optimization of Eq. (8). The result is given in Fig. 2. The optimal values that optimize Eq. (8) are four pair interactions constrained by $t=2$ and $\lambda=3$. The determination of

TABLE II. Directly calculated GGA formation enthalpies (meV/cation) for the input structures used to construct the cluster-expansion. In parentheses we give the fitted values given by CE. We have used in the GGA calculation a cutoff energy=300 eV, and **k**-point grid of $10\times10\times10$.

Formula	x_{Mn}	Directions (100)	(110)	(111)	(201)	(311)	Other Structures
Ga_7Mn_1	0.125						2x2x2 fcc supercell 26.14 (26.91)
Ga_3Mn_1	0.25	Z1 32.16 (31.70)	Y1 46.06 (44.22)	V1 28.74 (27.85)	DO_{22} 56.82 (57.57)	W1 40.24 (40.10)	$L1_2$ 55.70 (55.21)
Ga_2Mn_1	0.333	β1 35.08 (36.01)	γ1 53.68 (53.25)	α1 32.66 (35.56)			
Ga_1Mn_1	0.5	$L1_0$ 46.42 (46.01)		$L1_1$ 42.14 (40.78)			
Ga_2Mn_2	0.5	Z2 31.36 (31.06)	Y2 46.32 (46.46)	V2 23.26 (23.47)	CH 45.74 (45.98)	W2 41.94 (42.46)	

many-body interactions is done via a genetic algorithm. The evolution of S_{CV} of Eq. (6) with the number of generations is given in Fig. 3. Each point in this figure denotes a different many-body combination out of the pool of 57, which gives $\binom{57}{5}=4\,187\,106$ possible of such combinations. GA finds the optimal five-body combination with a minimum of $S_{CV}=1.98$ meV after 1310 generations. We run GA for 1690 more generations, to ensure that no better combinations of MBITs are found. The final interactions $\{J\}$ of Eq. (1) that fit best the GGA values and, at the same time, best predict the energies of structures not used in the fit [viz. Eq. (6)] are shown in Fig. 4. The first nearest-neighbor pair interaction is attractive (−28.47 meV), thus favoring the association of similar atoms, and is approximately 23 times larger than the remaining three repulsive pair interactions (second, third, and fourth nearest neighbors). The three-body interactions are repulsive and their magnitudes are approximately two and six times smaller than the attractive first nearest-neighbor pair interaction. The four-body interactions are all attractive and, on average, six times smaller than the first pair interaction.

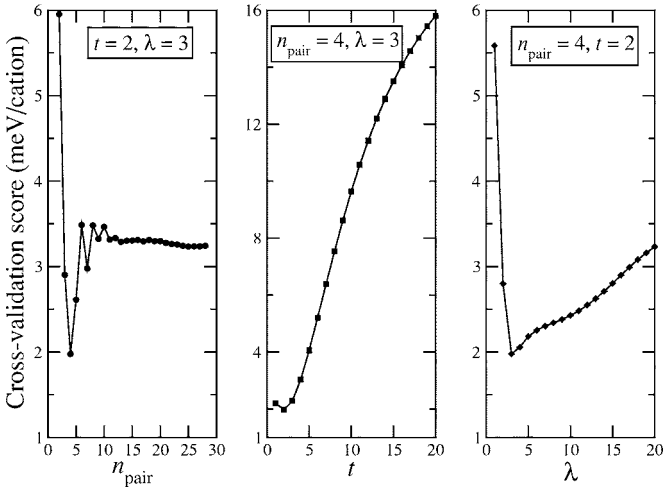

FIG. 2. Cross-validation score as a function of number of pairs n_{pair} and t and λ parameters [see Eq. (8)].

B. Prediction ability

We test the CE in five cases.

(a) The quality of the *fit* is shown in Table II via the numbers in parentheses, which give the CE-predicted ΔH_{CE}. The fitting error S_{fit} is defined by

$$S_{fit}=\sqrt{\frac{\sum_{\sigma=1}|\Delta\tilde{H}_{GGA}(\sigma)-\Delta\tilde{H}_{CE}(\sigma)|^2}{N_M}}. \qquad (11)$$

For $N_M=19$ input structures (17 in Table II plus GaAs and MnAs), $S_{fit}=0.97$ meV/cation. The maximum fitting error is 2.9 meV/cation, which is found for the $\alpha1$ structure.

(b) The quality of "pure predictions" is shown in

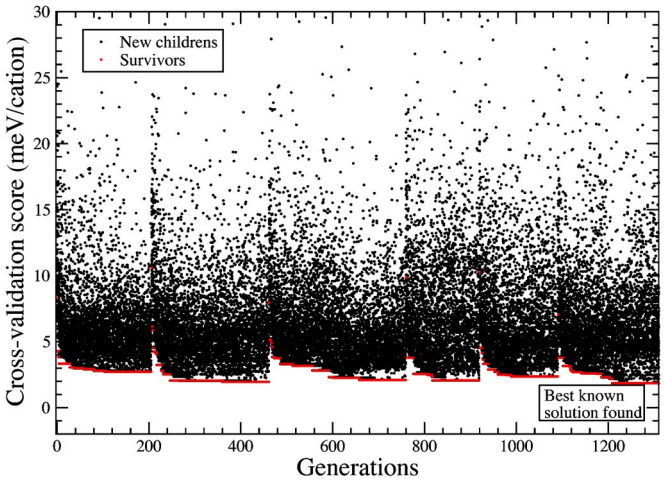

FIG. 3. (Color online) Cross-validation (CV) score, Eq. (6), history versus number of generations. The CV is minimized in 1310 generations.

Table I. The prediction error $S_{\text{pred.}}$ is defined by

$$S_{\text{pred.}} = \sqrt{\frac{\sum_{\sigma=1} |\Delta\tilde{H}_{\text{GGA}}(\sigma) - \Delta\tilde{H}_{\text{CE}}(\sigma)|^2}{N_V}}, \qquad (12)$$

for the $N_V=9$ predicted structures in Table I, with lattice constant $\bar{a}=5.750\,25$ Å, the $S_{\text{pred.}}=1.34$ meV/cation. The structure with the highest prediction error is the simple cubic 64 atoms supercell, where the two Mn atoms are first nearest neighbors, being 1.95 meV/cation.

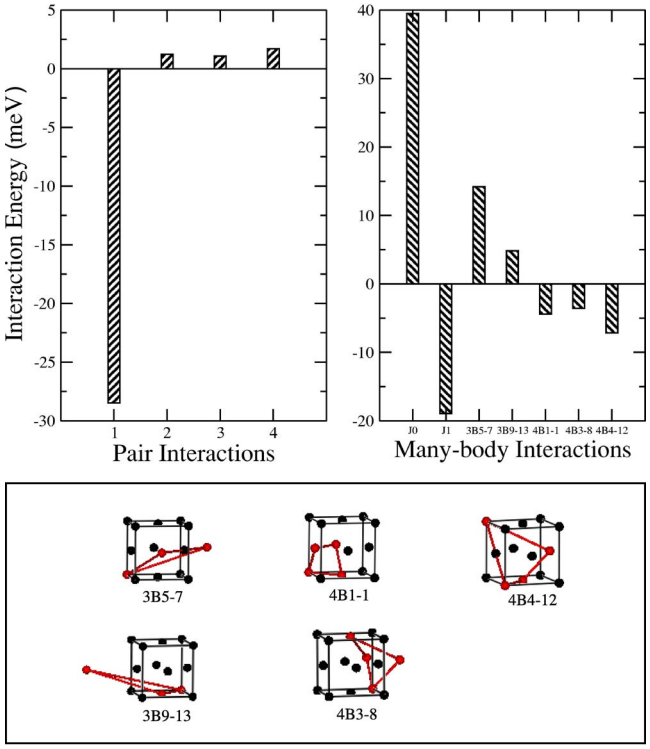

FIG. 4. (Color online) Pair and many-body interactions energies for the converged cluster expansion of the GaAs-MnAs system. The geometry of the converged many-body figures is shown on the bottom.

(c) To further test our CE, we constructed a complex structure, calculated its energy via the CE, and then compared it with a direct GGA calculation on this structure. The structure selected was $Ga_{56}Mn_8As_{64}$ with randomly placed Mn atoms in a $4\times4\times4$ supercell and lattice constant $\bar{a}=5.750\,25$ Å. We obtained $\Delta H_{\text{CE}}=29.04$ meV, $\Delta H_{\text{GGA}}=27.45$ meV.

(d) Another test is given by a special quasirandom structure[32] (SQS). We have used $Ga_6Mn_2As_8$ SQS-14, which is formally a $(GaAs)_6(MnAs)_2$ (301) superlattice, with lattice constant $\bar{a}=5.750\,25$ Å. For this structure, the values of $\bar{\Pi}_{\text{pair}}$ for the first and third pair are exactly equal to the corresponding value in a perfectly random $Ga_{0.75}Mn_{0.25}As$ alloy. To do so we first calculated the energy of a random alloy by analytically averaging on $\Delta H_{\text{CE}}(\sigma)$,

$$\Delta H_{\text{rand}}(x) = \langle \Delta H_{\text{CE}}(\sigma) \rangle. \qquad (13)$$

We compare this result to direct GGA using the SQS. We obtain $\Delta H_{\text{CE}}=41.32$ meV, $\Delta H_{\text{GGA}}=40.04$ meV.

(e) This CE has been constructed for concentrations $x \leqslant 0.5$, but we have tested it for zincblende $Ga_{1-x}Mn_xAs$ structures at higher concentrations x, specifically for the case of the superlattices $(GaAs)_1/(MnAs)_3$ along the (100) and (110) orientations (Z3 and Y3, respectively). For Z3 we obtain $\Delta H_{\text{CE}}=22.33$ meV, $\Delta H_{\text{GGA}}=23.00$ meV. In the case of Y3 we get $\Delta H_{\text{CE}}=30.00$ meV, $\Delta H_{\text{GGA}}=32.04$ meV.

The comparisons $(a)-(e)$ show that our CE is accurate to approximately 2 meV, even for structures not used in the fit, and even for the structures beyond the concentration range for which the CE was constructed.

C. The random alloy

The dashed line in Fig. 5 gives the mixing enthalpy of the random $Ga_{1-x}Mn_xAs$ alloy calculated from Eq. (13). Note its asymmetry with respect to $x=0.5$ due to odd-body interactions. We can fit Eq. (4) with $\Omega_1=293$ meV, $\Omega_2=-390$ meV, and $\Omega_3=239$ meV. We calculate the spinodal line from Eq. (4) using the mean field approximation for the free energy of mixing[33] $Ga_{1-x}Mn_xAs$

$$\Delta G(x) = \Omega_1 x(1-x) + \Omega_2 x^2(1-x) + \Omega_3 x^3(1-x) + k_B T[x\ln(x) + (1-x)\ln(1-x)], \qquad (14)$$

where k_B is the Boltzmann constant. The $\partial^2 \Delta G(x)/\partial x^2$ spinodal line is shown in Fig. 6. We see strong asymmetry in the T vs x spinodal line having two humps, implying a nontrivial phase diagram. Also, this asymmetry reflects the fact that Mn substitution in GaAs is energetically more costly than Ga substitution in zincblende MnAs. The miscibility-gap temperature at the maximum of the spinodal line is $T_{\text{MG}}=1348$ K at $x=0.204$. The typical growth temperature[2,5] of random $Ga_{1-x}Mn_xAs$ alloys are between 200 to 400 K, thus well inside the immiscible region, demonstrating that currently grown samples are well outside equilibrium.

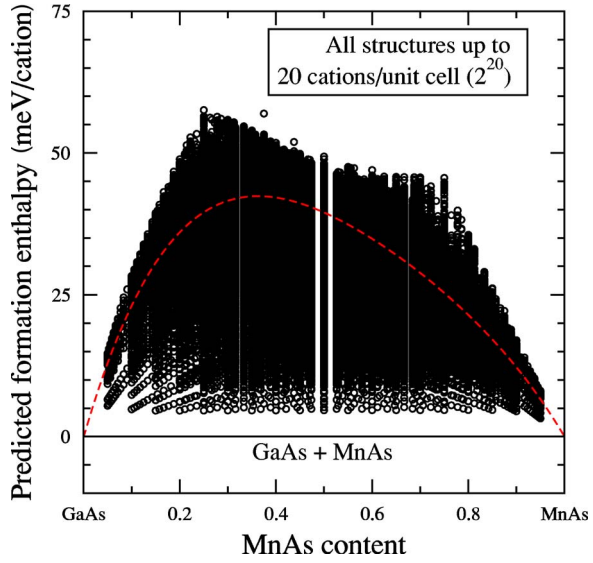

FIG. 5. (Color online) 2^{20} ground state structures up to 20 cations/unit cell. The dashed line is the mixing enthalpy of the random alloy.

D. $T=0$ ground state structures from exhaustive search

Having demonstrated a stable converged CE, we now evaluate from the CE the energies of all $Ga_nMn_mAs_{n+m}$ compounds up to $N=n+m\leqslant 20$ cations/cell. This is an exhaustive search of this space, which includes $\approx 3\times 10^6$ ordered compounds. Figure 5 shows the results, where each circle denotes a different structure and the dashed line denotes the random alloy. We see that the ground state line (the horizontal line in Fig. 5) corresponds to phase separation into GaAs+MnAs.

E. Superlattices

It is interesting to examine which of the structures of Fig. 5 is the least unstable. We therefore use the CE to calculate the energies of short-period superlattices (SLs). The results

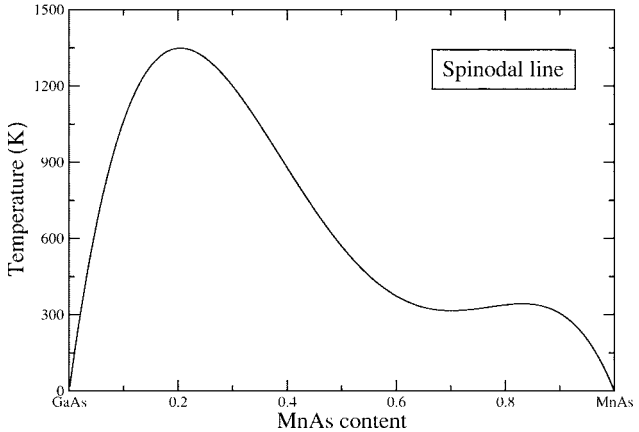

FIG. 6. Calculated spinodal line of $Ga_xMn_{1-x}As$ using mean-field approximation. The miscibility-gap temperature at the maximum of the spinodal line is $T_{MG}=1348$ K at $x=0.204$; below this temperature the alloy phase separates.

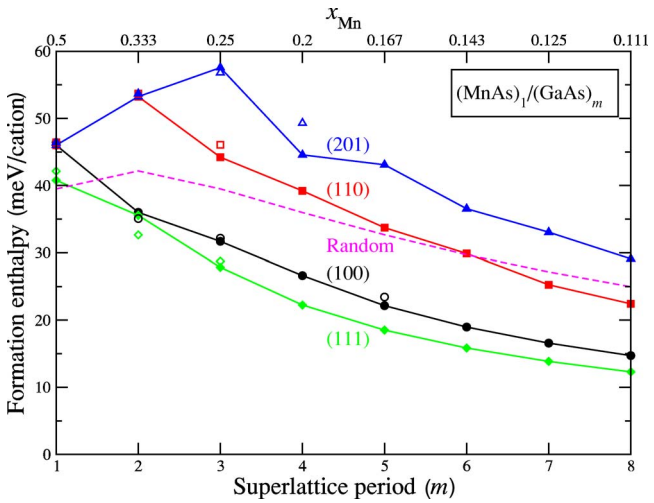

FIG. 7. (Color online) The formation enthalpy/cation versus the superlattice period of $(MnAs)_1/(GaAs)_m$ along the (100), (110), (111), and (201) orientations. Open circles, squares, diamonds, and triangles are direct GGA values for (100), (110), (111), and (201), respectively. The random alloy is denoted by a dashed line.

are shown in Fig. 7. For long periods, we see the order of stability given by Eq. (3). This reflects the order of interfacial energies $I(\hat{\mathbf{G}})$, since $\Delta H_{n,m}(\hat{\mathbf{G}})\rightarrow 2I(\hat{\mathbf{G}})/(n+m)$ for long periods. Calculated $I(\hat{\mathbf{G}})$ from $(n+m)\Delta H_{n,m}(\hat{\mathbf{G}})$ are shown in Fig. 8. We see that there is a critical value m_c such that $I(\hat{\mathbf{G}})$ becomes constant for longer periods $m>m_c$. The critical values are $m_c=3$ for the (111), $m_c=4$ for the (100), $m_c=5$ for the (110), and $m_c=6$ for the (201) orientation. The calculated interfacial energies for $(MnAs)_1/(GaAs)_m$ are $I(111)=111$ meV, $I(100)=133$ meV, $I(110)=202$ meV and $I(201)=256$ meV, giving

$$I(111)<I(100)<I(110)<I(201). \tag{15}$$

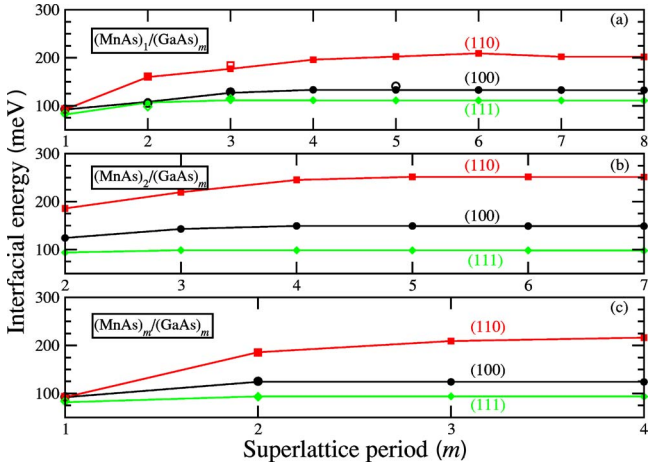

FIG. 8. (Color online) The interfacial energy versus superlattice period of $(MnAs)_n/(GaAs)_m$ along the (100), (110), and (111) orientations. The (a) $n=1$, (b) $n=2$, and (c) $n=m$. Open circles, squares, and diamonds are GGA values for (100), (110), and (111), respectively.

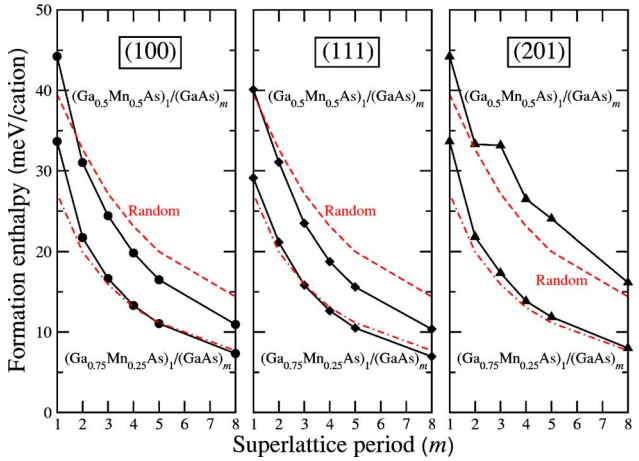

FIG. 9. (Color online) The formation enthalpy/cation versus superlattice period of $(Ga_{0.5}Mn_{0.5}As)_1/(GaAs)_m$ and $(Ga_{0.75}Mn_{0.25}As)_1/(GaAs)_m$ along the (100), (111), and (201) orientations. The random alloy is denoted by a dashed line and a dotted-dashed line at the same compositions that $(Ga_{0.5}Mn_{0.5}As)_1/(GaAs)_m$ and $(Ga_{0.75}Mn_{0.25}As)_1/(GaAs)_m$, respectively.

Comparing the formation enthalpies of $(MnAs)_1/(GaAs)_m$ SLs to the bulk random alloy of the same composition (Fig. 7), we find that SLs along (100) and (111) orientation are lower in energy than the random alloy when the thickness of the GaAs spacer between MnAs layers is $m \geq 2$. This is also so for the (110) orientation when $m \geq 7$ and for the (201) orientation when $m \geq 11$. Thus, once formed, these superlattices will not disorder at low T. Further, we calculate the formation enthalpies of alloy SL $(Ga_xMn_{1-x}As)_1/(GaAs)_m$ with $x=0.5, 0.25$ and $m=1,\ldots,8$, along the orientations (100), (111), (201). The results are shown in Fig. 9. We

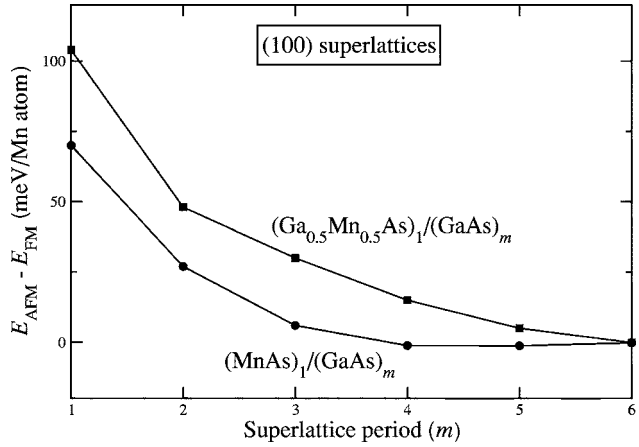

FIG. 10. Ferromagnetic stabilization energy of $(Ga_xMn_{1-x}As)_1/(GaAs)_m$ superlattices with a different intralayer Mn concentration.

observe that Eq. (3) still holds and, as expected, the decrease of intralayer Mn concentration tends to lower the energy. When these alloy SLs are compared to the random alloy, we observe that the formation enthalpies of $(Ga_{0.5}Mn_{0.5}As)_1/(GaAs)_m$ SLs are lower than the random alloy when $n \geq 2$ for the (100) and (111) orientations and $n \geq 11$ for the (201) orientation. The formation enthalpy of the random alloy and the $(Ga_{0.75}Mn_{0.25}As)_1/(GaAs)_n$ SLs are comparable.

F. Electronic structure and magnetism of superlattices

Having established the *chemical energetics* of superlattices, we next turn to study their magnetic properties. Figure 10 shows the energy difference $E_{AFM}-E_{FM}$ for two series of SLs: One with *concentrated* Mn in the layer, i.e.

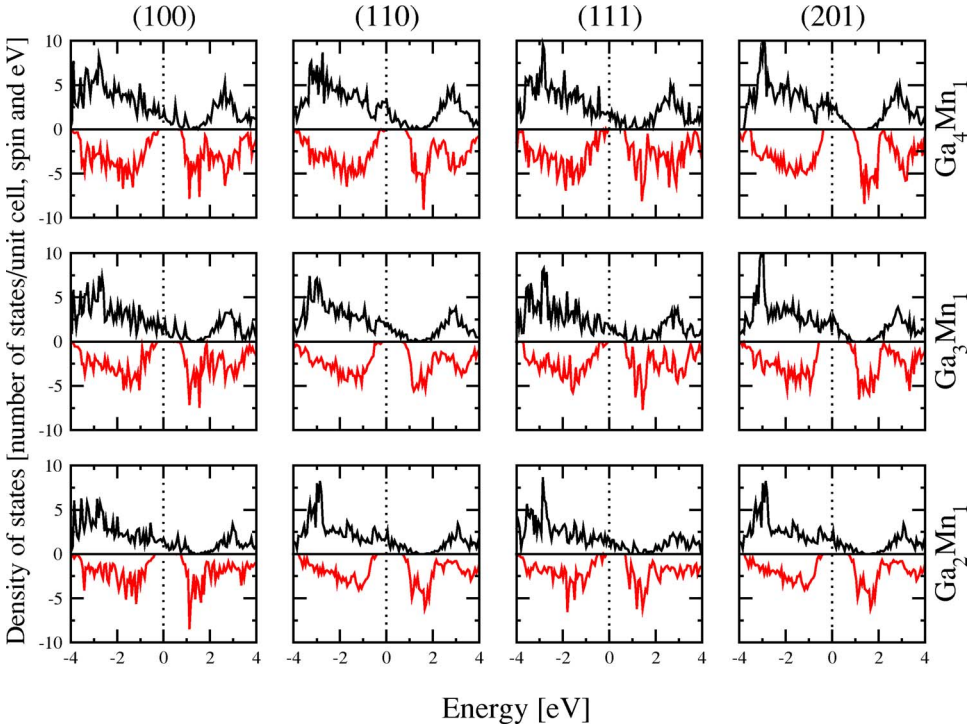

FIG. 11. (Color online) Total density of states for $(MnAs)_1/(GaAs)_m$ superlattices along the (100), (110), (111), and (201) orientations. The Fermi level is denoted by a vertical dotted line.

$(MnAs)_1/(GaAs)_n$, and one with more dilute Mn, i.e. $(Mn_{0.5}Ga_{0.5}As)_1/(GaAs)_n$. Interestingly, while the FM stabilization energy decreases with increasing the interlayer separation n, the decrease is much slower for the *dilute* SL. Thus, as we dilute Mn, the exchange interactions become longer range. This reveals an exceptional property of dilute magnetic semiconductors, namely that the system counterbalances dilution of the magnetic ions by extending the range of exchange interactions, hence maintaining ferromagnetism down to small concentrations of magnetic ion.

Figure 11 gives the total density of states (DOS) of the ferromagnetic short-period SLs. It is observed that all these SLs are half-metals, and the total magnetic moment per Mn atom is $4\mu_B$. The DOS shape is similar for the (100), (110), and (111) orientations. As the SL period increases from $(GaAs)_2(MnAs)_1$ to $(GaAs)_4(MnAs)_1$, the Fermi level moves toward the highest occupied state of the minority spin band. But along the (201) orientation the Fermi level shifts upward and then downward when the SL period is increased. Also, for the (201) orientation, the spin-up channel behaves differently from the the other three orientations: At higher energies above the Fermi level a bandgap larger than 0.3 eV takes place, which is increasing in value if the SL period is increased. We can also see that the spin-down bandgap (E_g) decreases with increasing the SL period for the (100), (110), and (111) orientations, but the gap increases for SL with the (201) orientation. Furthermore, the Mn $3d$ states exchange splitting (Δ_x) of these short-period SLs follows Eq. (3), where Δ_x for the (201) SLs are, on average, 0.5 eV larger than $\Delta_x$for the (111) SLs.

IV. SUMMARY

It is found that the ground state of the GaAs-MnAs system is phase separating into GaAs+MnAs. The formation enthalpy of short-period superlattices follows the order $(111)<(100)<(110)<(201)$, which implies that short-period superlattices along the (111) orientation are energetically more favorable thermodynamically. Note, however, that in vapor phase growth the control is kinetic, so all SLs are, in principle, growable. It is also found that the formation enthalpy of the random alloy becomes higher compared to superlattices in the dilute limit and therefore these superlattices will not disorder at low temperature. The calculated miscibility gap temperature is located at concentration $x\approx 0.2$. The stabilization energy for (100) $(Ga_{1-x}Mn_xAs)_1/(GaAs)_n$ superlattices shows that these superlattices prefer ferromagnetic order over a nonferromagnetic arrangement. The decay of the exchange interactions with superlattice period n is slower for the Mn dilute $x=0.5$ case than for $x=1$. This shows that as the system becomes more Mn-dilute the range of the exchange interactions increase.

ACKNOWLEDGMENTS

This work was funded by the ONR under NREL Contract No. DE-AC36-99GO10337.

*Electronic address: alex_zunger@nrel.gov
URL: www.sst.nrel.gov

[1] H. Ohno, H. Munekata, T. Penney, S. von Molnár, and L. L. Chang, Phys. Rev. Lett. **68**, 2664 (1992).
[2] Y. Ohno, D. K. Young, B. Beschoten, F. Matsukura, H. Ohno, and D. D. Awschalon, Nature **402**, 790 (2000).
[3] H. Ohno, D. Chiba, F. Matsukura, T. Omiya, E. Abe, T. Dietl, Y. Ohno, and K. Ohtani, Nature **408**, 944 (2000).
[4] R. K. Kawakami, E. Johnston-Helperin, L. F. Chen, M. Hanson, J. S. Speck, A. C. Gossard, and D. D. Awschalom, Appl. Phys. Lett. **77**, 2379 (2000).
[5] G. Kioseoglou, S. Kim, Y. L. Soo, X. Chen, H. Luo, Y. H. Kao, Y. Sasaki, X. Liu, and J. K. Furdyna, Appl. Phys. Lett. **80**, 1150 (2002).
[6] A. M. Nazmul, S. Sugahara, and M. Tanaka, Phys. Rev. B **67**, 241308(R) (2003).
[7] E. Johnston-Helperin, J. A. Schuller, C. S. Gallinat, T. C. Kreutz, R. C. Myers, R. K. Kawakami, H. Knotz, A. C. Gossard, and D. D. Awschalom, Phys. Rev. B **68**, 165328 (2003).
[8] K. H. Lee, H. J. Kim, J. C. Choi, H. Park, and T. W. Kim, J. Cryst. Growth **270**, 174 (2004).
[9] I. Vurgaftman and J. R. Meyer, Phys. Rev. B **64**, 245207 (2001).
[10] S. Sanvito, Phys. Rev. B **68**, 054425 (2003).
[11] Y. Ohishi, K. Sato, and H. Katayama-Yoshida, J. Magn. Magn. Mater. **272-276**, 1989 (2004).
[12] J. Hong, D. S. Wang, and R. Q. Wu, Phys. Rev. Lett. **94**, 137206 (2005).
[13] J. Ihm, A. Zunger, and M. L. Cohen, J. Phys. C **12**, 4409 (1979).
[14] Even though vapour-phase growth of superlattices is kinetically controlled (as evidenced by the fact that structures with positive formation enthalpies are made), it is of interest to establish which structure is least unstable.
[15] A. Zunger, in *Statics and Dynamics of Alloy Phase Transformations*, edited by P. E. A. Turchi and A. Gonis (Plenum, New York, 1994), Vol. 319 of Proceedings of the NATO Advanced Study Institute, Series B: Physics, p. 361.
[16] A. Zunger, L. G. Wang, G. L. W. Hart, and M. Sanati, Modell. Simul. Mater. Sci. Eng. **10**, 685 (2002).
[17] D. B. Laks, L. G. Ferreira, S. Froyen, and A. Zunger, Phys. Rev. B **46**, 12587 (1992).
[18] J. W. D. Connolly and A. R. Williams, Phys. Rev. B **27**, R5169 (1983).
[19] G. T. Rado and H. Suhl, in *Magnetism* (Academic, New York, 1965), Vol. 2B.
[20] C. Domb, in *Phase Transitions and Critical Phenomena*, edited by C. Domb and H. S. Green (Academic, London, 1974), Vol. 3, p. 357.
[21] D. M. Burley, in *Phase Transitions and Critical Phenomena*, edited by C. Domb and H. S. Green (Academic, London, 1972), Vol. 2, p. 329.
[22] D. F. Styer, M. K. Phani, and J. L. Lebowitz, Phys. Rev. B **34**, 3361 (1986).
[23] V. Blum and A. Zunger, Phys. Rev. B **70**, 155108 (2004).
[24] G. L. W. Hart, V. Blum, M. J. Walorski, and A. Zunger, Nat. Mater. **4**, 391 (2005).
[25] A. Zunger and S. Mahajan, in *Handbook of Semiconductors*

(Elsevier, Amsterdam, 1994), Vol. B, p. 1399.
[26] R. G. Dandrea, J. E. Bernard, S.-H. Wei, and A. Zunger, Phys. Rev. Lett. **64**, 36 (1990).
[27] A. Zunger, in *Handbook of Crystal Growth*, edited by D. J. Hurl (Elsevier, Amsterdam, 1994), Vol. 3, p. 997.
[28] V. Ozoliņš, C. Wolverton, and A. Zunger, Phys. Rev. B **57**, 4816 (1998).
[29] L. G. Ferreira, S.-H. Wei, and A. Zunger, Phys. Rev. B **40**, 3197 (1989).
[30] A. van de Walle and G. Ceder, J. Phase Equilib. **23**, 348 (2002).
[31] V. Blum, G. L. W. Hart, M. J. Walorski, and A. Zunger, unpublished.
[32] A. Zunger, S.-H. Wei, L. G. Ferreira, and J. E. Bernard, Phys. Rev. Lett. **65**, 353 (1990).
[33] I. Ho and G. B. Stringfellow, Appl. Phys. Lett. **69**, 2701 (1996).